Structure of the Pacinian Corpuscle: Insights Provided by Improved Mechanical Modeling

Ian R. Summers, Svetlana Pitts-Yushchenko, and C. Peter Winlove

Abstract—An improved model of the Pacinian corpuscle includes corrections for lamellar curvature. Results suggest that outer-zone lamellae produce a focusing effect whereby stimuli are channeled radially inwards. The requirements for this effect (large outer-surface area and thin, closely spaced lamellae) provide a rationale for the complexity of the outer-zone structure.

Index Terms—Biomechanics, mechanoreceptors, Pacinian corpuscle, touch perception

---◆---

1 INTRODUCTION

PACINIAN corpuscles (PCs) are one of several types of mechanoreceptor found in human skin [1], [2], [3]. They are also present in joints, muscles and other organs. PCs are also found in other mammals, in similar locations. Their shape typically approximates to a prolate spheroid, around 1 mm long. They have a characteristic layered structure in which a central core is surrounded by an outer zone, composed of a series of around 30 lamellae [4], [5], [6]. These lamellae are separated by fluid-filled spaces, within which there is a sparse network of collagen fibrils that appears to stabilize the structure. Each lamella is composed of living cells and supported by collagenous layers on its inner and outer surfaces. A nerve runs from the central core. Transduction from mechanical to electrical signals occurs in the region of the nerve ending, mediated by stretch-activated ion channels [7], [8]. PCs are highly sensitive to mechanical inputs in the frequency range 100 to 500 Hz [9], [10], and are believed to contribute significantly to the tactile sensations involved in manipulative tasks, e.g., sensations of surface texture [11]. Because of this, some virtual-touch devices have been designed specifically to stimulate PCs (e.g., [12], [13], [14]).

PCs are classified as "rapidly adapting" mechanoreceptors [15], i.e., they respond primarily to transients in a mechanical stimulus. This behavior can be attributed to their outer-zone structure, whose deformation rate is limited by resistance to fluid flow in the interlamellar spaces – the structure is rigid in response to a sudden transient but deformable in response to a steady pressure. In signal-processing terms, the outer zone behaves as a high-pass filter for displacement. Mechanical-to-electrical transduction at the nerve ending contributes a further low-pass response [16], giving a band-pass response for the PC as a whole. This band-pass response can be seen, for example, in measurements of the human tactile threshold on the hand [9], [10], [17]. In the frequency range 100 to 500 Hz, the threshold is dominated by the PC response and shows a peak in sensitivity at around 250 Hz.

This paper focuses on the fall-off in sensitivity at low frequencies which, as outlined above, can be attributed to the mechanical

behavior of the outer-zone of the PC. Pawson et al. [5], using recordings of nerve firing rate, measured an average fall-off of 12.0 dB/octave for PCs in the foot pad of the cat, and 12.7 dB/octave for PCs excised from the cat mesentery. Similar results from PCs in the cat mesentery were obtained by Bolanowski and Zwislocki [18]. In experiments on the human hand, measuring the vibrotactile threshold at frequencies for which the PC response dominates, Verrillo [9], [17] also measured a low frequency fall-off close to 12 dB/octave. (The modeling by Biswas et al. [16] suggests that the overlying tissue in the hand has little effect on the overall frequency response, and hence these results represent the response of the PCs themselves.) Comparing human psychophysical data and feline electrophysiological data, Verrillo [19] again observed a fall-off close to 12 dB/octave, in each case. The fact that these measured values are all very close to the 12 dB/octave fall-off of a second-order filter (i.e., a response proportional to frequency squared) suggests that there may be something intrinsic to the mechanical behavior of PCs which leads to such a response.

There is a lack of experimental data from direct measurements of mechanical transmission in the PC. Author SP-Y has measured sinewaves passing through an excised equine PC [20], producing a video which is included in the supplementary material for this paper. The PC was held between a stationary plate and a vibrating plate and the motion of the outer-zone lamellae was recorded, providing data which inform the choice of some model parameters in the present paper (see below, Section 2.2).

As outlined above, the observed low-frequency fall-off can be attributed to the outer-zone structure of the PC. However, it would be possible to obtain a second-order fall-off with a much simpler structure – a suitable combination of two compliant elements and two resistive elements. The existing literature provides no satisfactory explanation for the complexity of the outer-zone structure, with around 30 compliant elements (the lamellae) and 30 resistive elements (the fluid-filled interlamellar spaces). The mechanical modeling in the present paper provides some insights into this problem, giving a rationale for the structure of the outer zone. In addition, the modeling suggests that the outer zone functions to "focus" mechanical stimuli onto the central core, providing amplification as well as high-pass filtering.

For convenience of modeling, the spheroidal shape of the PC may be simplified to a sphere or a cylinder. In a recent paper, Quindlen et al. [21] use a PC model with a spherical geometry and obtain a surface-to-core displacement transfer function which has a peak in response at around 100 Hz and a response minimum at around 25 Hz. The modeling in the present paper uses a cylindrical geometry, and takes as a starting point the previous work of Loewenstein and Skalak [22] and Biswas et al. [23].

2 MODELING

This section outlines the model used in a previous study [22] and presents a new model with an improved treatment of fluid movement. Both models are based on a simplified geometry [22] in which the outer-zone structure of the PC is represented by a series of concentric cylindrical shells around a cylindrical core (Fig. 1). The network of collagen fibrils in the interlamellar spaces is modeled as numerous springs, which run radially between neighboring lamellae (not shown in Fig. 1). Further details of the assumptions made in this representation are given in the paper by Loewenstein and Skalak [22].

For both models, the analysis involves consideration of the distortion of the outer-zone structure in response to a pressure distribution on the PC surface, such that the ith lamella is subject to a radial displacement w_i (defined as positive inwards) of the form
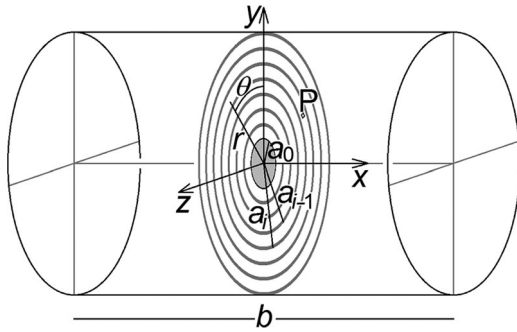
Fig. 1. Schematic diagram of the PC model, showing a central cross section through the set of lamellae in the form of concentric cylindrical shells. For clarity, only seven lamellae are shown. The lamellae surround a cylindrical central core. Position is represented by Cartesian coordinates x, y, z, or cylindrical polar coordinates x, r, θ. The overall length is b. The (outer) radius of the ith lamella (counting from the central core) is a_i; the radius of the inner core is a_0. The thickness of the ith lamella is d_i (not labelled in the diagram); the spacing between the $(i-1)$th and ith lamellae is h_i (not labelled in the diagram), where $h_i = a_i - a_{i-1} - d_i$. The representative point P is referred to in Section 3.2.

$$w_i = B_i \cos(2\theta)\cos(\pi x/b) \tag{1}$$

where B_i represents the overall magnitude and time variation of the displacement, and the $\cos(2\theta)$ variation corresponds to a change in the lamella diameter in the y direction and an equal and opposite change in in the z direction; these changes have their maximum magnitudes at the central cross section ($x = 0$) and fall to zero at the ends of the corpuscle ($x = \pm b/2$).

Data from the new model (and, for comparison, some recalculated data from the previous model) were obtained by implementing electrical analogs, in which electrical resistance and capacitance represent mechanical resistance and compliance [22], using *LTspice* software (Linear Technology Corporation).

2.1 Loewenstein and Skalak Model (L&S Model)

Loewenstein and Skalak [22] consider forces between the $(i-1)$th and ith lamellae of two types: elastic forces from the radial springs which link the lamellae, proportional to the relative displacement $w_i - w_{i-1}$, and resistive forces due to fluid flow in the interlamellar space, proportional to the time derivative of the relative displacement $\dot{w}_i - \dot{w}_{i-1}$. This analysis leads to the following equation, coupling the motion of neighboring lamellae:

$$w_i/K_i = R_{i+1}(\dot{w}_{i+1} - \dot{w}_i) + (w_{i+1} - w_i)/\kappa_{i+1} \\ - R_i(\dot{w}_i - \dot{w}_{i-1}) - (w_i - w_{i-1})/\kappa_i \tag{2}$$

where the first and third terms on the right-hand-side are the pressures on the ith lamella from its neighbors that derive from resistive forces, and the second and fourth terms are pressures that derive from elastic forces. The sum of these four terms gives the net pressure on the ith lamella, represented on the left-hand-side of the equation by the quotient of the displacement w_i and the compliance K_i of the ith lamella. R_i is the effective resistance due to viscous effects in the interlamellar space between the $(i-1)$th and ith lamellae; κ_i is the compliance due to the radial springs between the $(i-1)$th and ith lamella. Substituting into (2) from (1) and canceling gives

$$B_i/K_i = R_{i+1}(\dot{B}_{i+1} - \dot{B}_i) + (B_{i+1} - B_i)/\kappa_{i+1} \\ - R_i(\dot{B}_i - \dot{B}_{i-1}) - (B_i - B_{i-1})/\kappa_i. \tag{3}$$

If the effective Young modulus of the lamella membrane is E_m, the effective Young modulus of the assembly of radial springs is E_s, and the effective viscosity of the interlamellar fluid is μ, it can be shown [22] that:

$$K_i = a_i^2 \left(1 + 4b^2/\pi^2 a_i^2\right)^2 / E_m d_i \tag{4}$$

TABLE 1
Model Parameters

radius a_0 of central core	20.0 μm
outer radius a_1 of 1st lamella	21.8 μm
outer radius a_{30} of 30th lamella	250.0 μm
overall length b of model system	1000 μm
thickness d_i of ith lamella	0.25 μm
viscosity μ of interlamellar fluid	0.005 Pa s
resistivity η of central core	0.5 Pa s
Young modulus E_c of central core	1250 Pa
Young modulus E_m of lamellae	10^5 Pa
Young modulus E_s of radial springs	10 Pa

$$R_i = 12\mu b^2/h_i^3 \pi^2 \left(1 + 4b^2/\pi^2 a_i^2\right) \tag{5}$$

$$\kappa_i = h_i/E_s \tag{6}$$

where additional symbols are defined in the Fig. 1 legend.

Loewenstein and Skalak [22] focused on the propagation of pressure in the PC and assumed the central core to be rigid. However, as mentioned above, transduction in the central core is now thought to be mediated by stretch-activated ion channels; consequently, the present paper focuses on the propagation of displacement. To obtain displacement data, the original L&S model [22] has been modified by assuming a non-rigid central core with an input compliance $K_0 = a_0/E_c$, where E_c is the effective Young modulus of the core. The input impedance of the core is assumed to have a resistive component also, of the form $R_0 = \eta/a_0$, where the resistivity η has the dimensions of viscosity. Data from the modified L&S model were calculated for comparison with the new model. To facilitate this comparison, the L&S model parameters have been updated to those used in the new model (see Section 2.2 and Table 1). Solutions of (3) model the way in which displacement propagates across the set of 30 lamellae, from the PC surface to the central core.

For basically the same model system (Fig. 1), with a viscoelastic central core, Biswas et al. [23] presented an analysis which takes account of the inertia of the various PC components. However, inertial effects were found to be negligible and thus their model (the BMS model) is very similar to the modified L&S model described in this section.

2.2 New Model

For the new model, again based on the system in Fig. 1, (3) is modified as follows:

(i) Equivalent radial movements $\dot{w}_{i-1}$ and $\dot{w}_i$ of the $(i-1)$th and ith lamellae do not produce exactly equal volume flows in the interlamellar space because of the difference in surface area between the lamellae: the lamella areas are in the ratio $S_{i-1}/S_i = a_{i-1}/a_i$, where $S_i = 2\pi a_i b$ is the surface area of the ith lamella. To take account of this, the volume flow produced by movement of the $(i-1)$th lamella is reduced by a factor $\sqrt{a_{i-1}/a_i}$ and the volume flow produced by movement of the ith lamella is increased by a factor $\sqrt{a_i/a_{i-1}}$, thus achieving the required relative weighting of a_{i-1}/a_i. The effect of this modification is small in the context of a single interlamellar space, but the cumulative effect over the set of lamellae is significant, giving an increase in overall gain by a factor of a_{30}/a_0, as shown below in Section 3.2.

(ii) Again because of the difference in lamella area, the radial springs between the $(i-1)$th and ith lamellae exert equal and opposite *forces* on the lamellae, but not exactly equal and opposite *pressures*. To take account of the change in area $(S_{i-1}/S_i = a_{i-1}/a_i)$, the pressure exerted on the $(i-1)$th lamella is increased by a factor $\sqrt{a_i/a_{i-1}}$ and the

pressure exerted on the ith lamella is reduced by a factor $\sqrt{a_{i-1}/a_i}$, thus achieving the required relative weighting of a_{i-1}/a_i. As in the L&S model, these pressures are proportional to the relative motion of the lamellae. (The radial springs determine the quasi-static behavior of the model, which is not the focus of interest here – this modification is included only for completeness.)

The modified (3) is as follows:

$$
\begin{aligned}
B_i/K_i =\, & R_{i+1}\Big(\sqrt{a_{i+1}/a_i}\ \dot{B}_{i+1} - \sqrt{a_i/a_{i+1}}\ \dot{B}_i\Big) \\
& + \sqrt{a_{i+1}/a_i}(B_{i+1} - B_i)/\kappa_{i+1} \\
& - R_i\Big(\sqrt{a_i/a_{i-1}}\ \dot{B}_i - \sqrt{a_{i-1}/a_i}\ \dot{B}_{i-1}\Big) \\
& - \sqrt{a_{i-1}/a_i}(B_i - B_{i-1})/\kappa_i
\end{aligned}
\tag{7}
$$

with K_i and κ_i as in (4) and (6), and R_i now given by a slightly modified version of (5), taking account of the difference in radius between the $(i-1)$th and ith lamellae:

$$
R_i = 12\mu b^2/h_i^3\pi^2\big(1 + 4b^2/\pi^2 a_{i-1}a_i\big).
\tag{8}
$$

Equation (7) can be rewritten as

$$
\begin{aligned}
a_i B_i/K_i' =\, & R_{i+1}'\big(a_{i+1}\dot{B}_{i+1} - a_i\dot{B}_i\big) + (a_{i+1}B_{i+1} - a_iB_i)/\kappa_{i+1}' \\
& - R_i'\big(a_i\dot{B}_i - a_{i-1}\dot{B}_{i-1}\big) - (a_iB_i - a_{i-1}B_{i-1})/\kappa_i'
\end{aligned}
\tag{9}
$$

where

$$
R_i' = R_i/\sqrt{a_{i-1}a_i}
\tag{10}
$$

$$
\kappa_i' = \kappa_i\sqrt{a_{i-1}a_i}
\tag{11}
$$

$$
1/K_i' = 1/a_iK_i + (a_{i+1} - a_i)/a_i\kappa_{i+1}' - (a_i - a_{i-1})/a_i\kappa_i'.
\tag{12}
$$

Equation (9) has the same form as (3) for the L&S model, but the variable B_i is replaced by a_iB_i.

The central core is again assumed to have an input compliance $K_0 = a_0/E_c$ and an input resistance $R_0 = \eta/a_0$, where E_c is the effective Young modulus and the resistivity η has dimensions of viscosity. For use in this model, the quantities K_0 and R_0 are transformed to quantities K_0' and R_0', using relations analogous to (10) and (12) which, to a good approximation, can be written as:

$$
K_0' = a_0K_0 = a_0{}^2/E_c
\tag{13}
$$

$$
R_0' = R_0/a_0 = \eta/a_0{}^2.
\tag{14}
$$

The model parameters are given in Table 1. Values for lamella radius are calculated using

$$
a_i = a_0\Big(12.5^{i/30}\Big)
\tag{15}
$$

where $a_0 = 20\ \mu$m. Equation (15) is a simplified version of the power law used by Loewenstein and Skalak [22], based on the analysis of Hubbard [24]. For convenience, since individual differences in lamella thickness are not important for the overall behavior of the model, the same value of 0.25 μm is assumed for the thickness d_i of each lamella. This value is in line with measurements by Chouchkov [25] and Malinovsky et al. [26].

It is difficult to provide an accurate estimate for the Young modulus E_m of the lamellae – it seems likely that the elastic behavior of a lamella is dominated by the collagenous layers on its inner and outer surfaces, which make up perhaps 10% of the overall lamella thickness d_i [6], [27], [28], but data on the relevant mechanical properties of these layers are not available. (It is known that their composition includes collagen IV and laminin [29].) A Young modulus of 10^6 Pa has been assumed for the collagenous layers, giving an effective Young modulus of 10^5 Pa for the lamella as a whole.
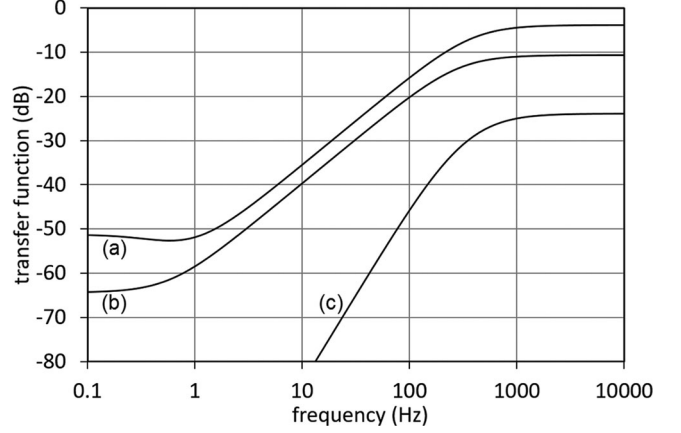

Fig. 2. Calculated displacement transfer functions: (a) from the new model, (b) from the modified L&S model, and (c) from the new model, including additional modeling of transmission within the central core.

This contrasts with the very low value of 1000 Pa assumed in the BMS model [23]. However, in practice the new model is not sensitive to the exact value of E_m; the lamella stiffnesses K_i are determined by E_m, but these have negligible effect on the displacement transfer function of the outer-zone structure as a whole – see below.

A value of 5 mPa s is assumed for the viscosity μ of the interlamellar fluid. This is within the range suggested by Biswas et al. [23].

As mentioned above, the radial springs determine the quasi-static behavior of the model, which is not the focus of interest here. A value of 10 Pa has been assumed for the Young modulus E_s of the radial springs, lying between the values used in the BMS model and the original L&S model. Values for the Young modulus E_c and resistivity η of the central core are chosen so that the high-pass response of the mechanical filter has a pass-band gain of approximately –4 dB and a 3-dB point close to 400 Hz. The gain at 400 Hz is thus around –7 dB, in line with the measurement by author SP-Y [20] of the transmission of a 400 Hz sinusoidal displacement through the PC outer zone. Solutions of (9) model the way in which displacement propagates across the set of 30 lamellae.

3 RESULTS AND DISCUSSION

3.1 Modeling Data

Fig. 2 shows graphs of surface-to-core transfer function as a function of frequency. Graph (a) shows the displacement transfer function $|B_0/B_{30}|$ for the new model, using the parameters shown in Table 1. The maximum slope in the fall-off region is 6.0 dB/octave, i.e., the model shows a first-order high-pass response at frequencies above 5 Hz. The 3-dB point is at 380 Hz. Below 5 Hz the transfer function flattens off, because of the effect of the radial springs which determine the quasi-static response. Graph (b), for the modified L&S model, using the same parameters, also shows a first-order high-pass response. The 3-dB point is at 282 Hz. Graph (c) relates to a modification of the new model, described in Section 3.3.

3.2 Model Response

Except at very low frequencies, the response of the new model is first-order because the radial-spring compliances κ_i' and the lamella compliances K_i' are sufficiently large for the behavior of the outer-zone structure to be entirely dominated by the interlamellar resistances R_i'. Since the only significant impedances in the outer-zone structure are resistances, these are effectively lumped together so that the whole structure behaves as a single resistance. The model then reduces to only three elements, as shown in Fig. 3a: a resistance R_{lam}' representing the outer-zone lamellar structure, given by

$$1/R'_{lam} = \sum_i (1/R'_i) \qquad (16)$$

together with the compliance K'_0 and resistance R'_0 representing the input impedance of the core.

The transfer function of this three-element system is

$$\left| \frac{B_0}{B_{30}} \right| = \frac{a_{30}}{a_0} \left(\frac{R'_{lam}}{R'_0 + R'_{lam}} \right) \left(1 + \left(\frac{f_{3dB}}{f} \right)^2 \right)^{-1/2} \qquad (17)$$

where f is frequency and f_{3dB} is the 3-dB-point frequency, given by

$$f_{3dB} = 1/2\pi K'_0 (R'_0 + R'_{lam}). \qquad (18)$$

As mentioned in the previous section, the modified L&S model also demonstrates a first-order fall-off. For this system also, the outer-zone structure behaves as a single lumped resistance, except at very low frequencies. The same is true for the BMS model [23]. For the modified L&S model, an expression similar to (17) may be derived; however, in that case the a_{30}/a_0 term is missing because the L&S model ignores the curvature of the lamellae when calculating fluid flow, and hence does not take account of the change in area across the set of lamellae.

At frequencies above 5 Hz, (17) gives a very close fit to the transfer function calculated using the full model (Fig. 2, graph (a)). In (17) and (18), R'_{lam} is proportional to μ, R'_0 is proportional η, and K'_0 is inversely proportional to E_c, indicating how the transfer function is affected by the particular choice of values for μ, η and E_c. For the model parameters given in Table 1, $R'_0/R'_{lam} = 18.5$; consequently, the 3-dB-point frequency given by (18) is largely determined by K'_0 and R'_0, i.e., by the properties of the central core.

From (17) it can be seen that the pass-band gain is the product of two factors. The first, a_{30}/a_0, represents the amplification associated with the "focusing" effect produced by the outer-zone structure: the motion of particles in the interlamellar fluid (e.g., a particle at point P in Fig. 1) is promoted in the radial direction, because the lamella compliances are sufficiently large for their effect to be negligible, and hindered in directions tangential to the lamellae, due to the dominant effect of the resistances in the interlamellar spaces. The factor a_{30}/a_0 arises because volume flow is conserved – for purely radial flow, displacement is inversely proportional to lamella area and hence inversely proportional to lamella radius a_i in this cylindrical geometry. For the model parameters given in Table 1, this factor a_{30}/a_0 evaluates to 12.5, equivalent to a gain of approximately 22 dB. This factor is not represented in the L&S or BMS models because these do not correctly demonstrate the conservation of volume flow. The improved treatment of fluid flow in the new model allows the conservation to be correctly represented, and hence allows an interpretation in terms of radial flow and focusing (see Section 3.4, below).

In fact, the flow is not purely radial: the mechanical load provided by the central core produces some "squeezing" of the interlamellar spaces, resulting in flow along these spaces. This is represented by the second factor in the pass-band gain: $R'_{lam}/(R'_0 + R'_{lam})$, from (17). This factor shows how only a fraction of the input stimulus at the PC surface is delivered to the central core, with the remainder being accommodated by distortion of the outer-zone structure. For the model parameters given in Table 1, this second factor evaluates to approximately 0.05, equivalent to a gain of –26 dB, giving an overall pass-band gain (both factors included) of –4 dB, as intended (see Section 2.2).

A comparison of graphs (a) and (b) in Fig. 2 shows the effect of incorporating the improved treatment of fluid flow in the new model. At first sight, it is surprising that the calculated transfer functions differ by only around 7 dB in the pass band, rather than the 22 dB associated with the first term (a_{30}/a_0) in the pass-band gain, from (17). This is because the discrepancy between the two
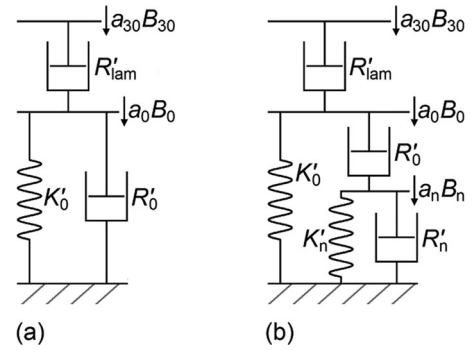

Fig. 3. (a) Simplified equivalent of the new model. (b) Simplified equivalent with additional components to represent transmission within the central core. The spring and dashpot symbols represent compliances and resistances.

models is reduced by the "squeezing" term in the pass-band gain, whose magnitude differs by 15 dB between the two models. (The discrepancy between the unity pass-band gain calculated for the BMS model [23] and the less-than unity pass-band gain shown in Fig. 2 for the modified L&S model can be attributed to differences in the viscoelastic representations of the core.)

3.3 Low Frequency Fall-Off

A significant deficiency of the new model is that it predicts a low-frequency fall-off of 6 dB/octave (see Section 3.1), i.e., a response proportional to frequency. This does not correspond to the 12 dB/octave fall-off seen in experimental studies, proportional to frequency squared. There are similar problems with the modified L&S model (Fig. 2, graph (b)) and the BMS model [23]. A steeper fall-off may in principle be obtained if the model parameters are chosen to give lower lamella compliances and/or lower interlamellar resistances, such that the effect of lamella compliance is not entirely negligible. However, in the new model, increasing the Young modulus E_m of the lamellae by a factor of 100 only changes the fall-off to around 7.5 dB/octave, and it would be very difficult to justify a greater change in the model parameters.

It is possible that a model with a spherical geometry might provide a better prediction of the low-frequency fall-off – Quindlen et al. [21], using a spherical model, calculate a low-frequency fall-off which is interrupted by a response minimum at around 25 Hz, and so again does not correspond well with the experimental data. (Their results may be affected by the incomplete specification of the central core in their model.)

Another possible explanation for the discrepancy between modeling and experimental results is that some mechanism in the central core might act as a further high-pass filter, providing an additional fall-off to that from transmission through the outer-zone structure, thus producing a 12 dB/octave fall-off overall. Such a mechanism might relate to the transduction from mechanical to electrical signals which occurs in the region of the nerve ending. (The results of Biswas et al. [16] may provide a suggestion of this.) Alternatively, the mechanism might relate to the transmission of displacement from the outer region of the central core to the nerve ending in its interior. For example, Fig. 3b shows a modified version of the model in Fig. 3a, in which the outer region of the central core, with compliance K'_0, is linked by a resistance R'_0 to the inner region of the central core, containing the nerve ending, which has input compliance K'_n and input resistance R'_n. Displacement of the inner region is represented by $a_n B_n$, where B_n is the displacement magnitude and a_n is an appropriate radius. The transfer function $|B_n/B_{30}|$ of such a system (PC surface to core inner region) is shown in Fig. 2, graph (c); the low-frequency fall-off is 12 dB/octave, as intended; for illustration, the model parameters are chosen to give a pass-band gain that is 20 dB lower than that in graph (a). Pawson et al. [30] observed a concentration of collagen V in the outer region of the central core; however, it must be stressed that

beyond this there is little anatomical evidence for the configuration shown in Fig. 3b; it is presented here as an example of how it may be possible to find a solution to the discrepancy between modeling and experiment.

3.4 Focusing and Amplification

The improved treatment of fluid flow in the new model affects the calculated transfer function, as shown in Fig. 2 and discussed above. However, the changes made in the new model are important not only because of this effect, but also for the insight that they bring to understanding the function of the outer zone of the PC. As mentioned in Section 3.2, the nature of the outer-zone structure is such that it produces a focusing effect – it allows radial movement of the interlamellar fluid and hinders flow in directions tangential to the lamellae. Displacement stimuli at the PC surface are channeled towards the core and this focusing effect is accompanied by an amplification of the displacement which tends to counteract the attenuation produced by resistive elements in the system, as shown by (17). This analysis suggests a resolution to an important and longstanding problem in understanding the mechanical behavior of the PC, providing a rationale for the complexity of the outer-zone structure, as follows: The outer surface of the PC defines a "catchment area" over which displacement stimuli are channeled towards the central core. A relatively large PC radius (compared, say, to the size of the nerve ending in the central core) provides a large catchment area, so that a single nerve can efficiently detect stimuli from a relatively large volume of tissue. The lamellae in the outer zone of the PC provide high-pass filtering and, because the focusing effect relies on high lamella compliances and high interlamellar resistances, they must be thin and closely spaced – Equations (4) and (5) indicate the effect of lamella thickness d_i and lamella spacing h_i on compliance and resistance. A large number of lamellae is now seen to be a consequence of the requirement for a large PC radius (to give a large catchment area) and the requirement for thin, closely spaced lamellae (to achieve the focusing effect).

4 CONCLUSIONS

By incorporating an improved description of fluid movement, the model presented in this paper provides new insights into the surface-to core displacement transfer function in the PC. Surprisingly, the multilayer structure appears to behave as only a single-stage filter. The lamella compliances are sufficiently large for the behavior of the outer-zone structure to be entirely dominated by the interlamellar resistances. Hence the outer-zone structure can be described by a single lumped resistance, and the transfer function is strongly dependent on the input compliance and resistance of the central core. The outer-zone structure produces a focusing effect, whereby displacement stimuli are channeled radially inwards from the catchment area of the PC surface towards the central core. In the light of this representation of the PC response, the previously unexplained complexity of the outer-zone structure can now be seen as a consequence of the advantage from the focusing effect (which relies on thin, closely spaced lamellae) and the advantage from a large catchment area (which requires a large PC radius). The model produces a first-order high-pass response with a low-frequency fall-off of 6 dB/octave, which does not match the 12 dB/octave fall-off seen experimentally – the origin of this deficiency in the model is not clear, but it may be explained in terms of additional high-pass filtering within the core. Further experimental measurements on PC response to vibratory stimuli, and on the mechanical properties of PC constituents, are required to inform the development of better models.

ACKNOWLEDGMENTS

REFERENCES

[1] T. A. Quilliam and J. Armstrong, "Mechanoreceptors," *Endeavour*, vol. 22, pp. 55–60, 1963.

[2] K. O. Johnson, T. Yoshioka, and F. Vega-Bermudez, "Tactile functions of mechanoreceptive afferents innervating the hand," *J. Clin. Neurophysiol.*, vol. 17, pp. 539–558, 2000.

[3] F. McGlone and D. Reilly, "The cutaneous sensory system," *Neurosci. Biobehav. Rev.*, vol. 34, pp. 148–159, 2009.

[4] J. Bell, S. Bolanowski, and M. H. Holmes, "The structure and function of Pacinian corpuscles," *Prog. Neurobiol.*, vol. 42, pp. 79–128, 1994.

[5] L. Pawson, C. M. Checkosky, A. K. Pack, and S. J. Bolanowski, "Mesenteric and tactile Pacinian corpuscles are anatomically and physiologically comparable," *Somatosens. Mot. Res.*, vol. 25, pp. 194–206, 2008.

[6] D. C. Pease and T. A. Quilliam, "Electron microscopy of the Pacinian corpuscle," *J. Biophys. Biochem. Cytol.*, vol. 3, pp. 331–342, 1957.

[7] L. Pawson and S. J. Bolanowski, "Voltage-gated sodium channels are present on both the neural and capsular structures of Pacinian corpuscles," *Somatosens Mot. Res.*, vol. 19, pp. 231–237, 2002.

[8] Y. Dong, S. Mihalas, S. S. Kim, T. Yoshioka, S. Bensmaïa, and E. Niebur, "A simple model of mechanotransduction in primate glabrous skin," *J. Neurophysiol.*, vol. 109, pp. 1350–1359, 2013.

[9] R. T. Verrillo, "Effect of contactor area on the vibrotactile threshold," *J. Acoust. Soc. Am.*, vol. 35, pp. 1962–1966, 1963.

[10] G. A. Gescheider, S. J. Bolanowski, and K. R. Hardick, "The frequency selectivity of information-processing channels in the tactile sensory system," *Somatosens. Mot. Res.*, vol. 18, pp. 191–201, 2001.

[11] M. Hollins, S. J. Bensmaïa, and S. Washburn, "Vibrotactile adaptation impairs discrimination of fine, but not coarse, texture," *Somatosens. Mot. Res.*, vol. 18, pp. 253–262, 2001.

[12] I. R. Summers and C. M. Chanter, "A broadband tactile array on the fingertip," *J. Acoust. Soc. Am.*, vol. 112, pp. 2118–2126, 2002.

[13] D. Allerkamp, G. Boettcher, F.-E. Wolter, A. C. Brady, J. Qu, and I. R. Summers, "A vibrotactile approach to tactile rendering," *Vis. Comput.*, vol. 23, pp. 97–108, 2007.

[14] M. Philpott and I. R. Summers, "Surface-roughness-based virtual textiles: Evaluation using a multi-contactor display," *IEEE Trans. Haptics*, vol. 8, no. 2, pp. 240–244, Apr.-Jun. 2015.

[15] M. Knibestöl, "Stimulus-response functions of rapidly adapting mechanoreceptors in the human glabrous skin area," *J. Physiol.*, vol. 232, pp. 427–452, 1973.

[16] A. Biswas, M. Manivannan, and M. A. Srinivasan, "Vibrotactile sensitivity threshold: Nonlinear stochastic mechanotransduction model of the Pacinian corpuscle," *IEEE Trans. Haptics*, vol. 8, no. 1, pp. 102–113, Jan.-Mar. 2015.

[17] R. T. Verrillo, "Vibrotactile thresholds measured at the finger," *Percept. Psychophys.*, vol. 9, pp. 329–330, 1971.

[18] S.J. Bolanowski and J.F. Zwislocki, "Intensity and frequency characteristics of pacinian corpuscles. I. Action Potentials," *J. Neurophysiol.*, vol. 51, pp. 793–811, 1984.

[19] R.T. Verrillo, "Vibrotactile sensitivity and the frequency response of the Pacinian corpuscle," *Psychonom. Sci.*, vol. 4, pp. 135–136, 1966.

[20] S. Pitts-Yushchenko, "Mechanisms of mechanotransduction in the pacinian corpuscle," Ph.D. dissertation, Univ. Exeter, Exeter, United Kingdom, 2013, pp. 142–146.

[21] J. C. Quindlen, H. K. Stolarski, M. D. Johnson, and V. H. Barocas, "A multiphysics model of the Pacinian corpuscle," *Integr. Biol.*, vol. 8, pp. 1111–1125, 2016.

[22] W. R. Loewenstein and R. Skalak, "Mechanical transmission in a Pacinian corpuscle. An analysis and a theory," *J. Physiol.*, vol. 182, pp. 346–378, 1966.

[23] A. Biswas, M. Manivannan, and M. A. Srinivasan, "Multiscale layered biomechanical model of the Pacinian corpuscle," *IEEE Trans. Haptics*, vol. 8, pp. 31–42, Jan.-Mar. 2015.

[24] S. J. Hubbard, "A study of the rapid mechanical events in a mechanoreceptor," *J. Physiol.*, vol. 141, pp. 198–218, 1958.

[25] C. N. Chouchkov, "Ultrastructure of Pacinian corpuscles in men and cats," *Z. Mikrosk. Anat. Forsch.*, vol. 83, pp. 17–32, 1971.

[26] L. Malinovsky, L. Pac, J. A. Vega-Alvarez, and W. Bozilow, "The capsule structure of Pacinian corpuscles from the cat mesentery," *Z. Mikrosk. Anat. Forsch.*, vol. 104, pp. 193–201, 1990.

[27] C. Ide, and S. Hayashi, "Specializations of plasma membranes in Pacinian corpuscles: implications for mechano-electric transduction," *J. Neurocytol.*, vol. 16, pp. 759–773, 1987.

[28] K. Sames, et al., "Lectin and proteoglycan histochemistry of feline Pacinian corpuscles," *J. Histochem. Cytochem.*, vol. 49, pp. 19–28, 2001.

[29] J.A. Vega, I. Esteban, F. J. Naves, M. E. del Valle, and L. Malinovsky, "Immunohistochemical localization of laminin and type IV collagen in human cutaneous sensory nerve formations," *Anat. Embryol.*, vol. 191, pp. 33–39, 1995.

[30] L. Pawson, N. B. Slepecky, and S. J. Bolanowski, "Immunocytochemical identification of proteins within the Pacinian corpuscle," *Somatosens. Mot. Res.*, vol. 17, pp. 159–170, 2000.